Research articles

Current-induced spin-orbit effective field modulations in synthetic antiferromagnetic structures

S. Krishnia, C. Murapaka, P. Sethi, W.L. Gan, Q.Y. Wong, G.J. Lim, W.S. Lew*

School of Physical and Mathematical Sciences, Nanyang Technological University, 21 Nanyang Link, Singapore 637371

A B S T R A C T

We demonstrate the modulation of spin-orbit torque (SOT) fields in synthetic antiferromagnetic (SAF) structures sandwiched between two heavy metals of opposite spin Hall angles. The SOTs fields that are measured by using harmonic Hall voltage technique, increase with net areal magnetization of the Pt/SAF/Ta structures. The result suggests an antiparallel orientation of the SOT fields in the two ferromagnetic layers. The antiparallel alignment of the SOT fields switches the magnetization of SAF structures with a current density as low as 2.3×10^{11} A/m^2.

Control on magnetization direction in ferromagnetic (FM) layers via spin-charge interactions is crucial step for realizing low-power, high-speed spintronic memory and logic devices [1–4]. In recent years, spin-orbit torques (SOTs) in FM materials, induced by charge-current flowing through adjacent heavy metals (HM) have emerged as an energy efficient and alternative route for magnetization manipulation [5–8]. In SOT devices, spin-current that is generated by spin Hall effect in the HM, diffuses into the adjacent FM layer and exerts torques: SOTs, on its magnetization. The efficiency of switching in the SOT devices is determined by the associated effective fields. So far, the investigation of current-induced effective fields are mostly limited to single FM layers with in-plane [9], perpendicular [10,11] and modulated magnetic anisotropies [12–15]. Recently, synthetic antiferromagnetic (SAF) structures where two FM layers are coupled antiferromagnetically via an ultrathin metallic layer, have been proven to be more reliable for device applications [16–19]. The SAF structures have been widely adopted in magnetic tunnel junctions to improve the thermal stability of magnetic random access memory (MRAM) devices [20,21]. The current-induced magnetization switching mechanism in such structures is complex and greatly influenced by antiferromagnetic coupling and applied magnetic field strengths [22,23]. More recently, SOT induced switching of SAF structures was reported in the presence of large in-plane magnetic fields. G. Y. Shi et al., have shown the simultaneous switching of two antiferromagnetically coupled CoFeB FM layers between two anti-parallel states via spin currents induced by SHE in Ta spacer layer [23]. C. Bi et al., have reported anomalous SOT induced switching behaviour in SAF structures due to asymmetric domain wall motion [22]. However, the quantification of current-induced effective fields in the SAF heterostructures still remains elusive. Here, we have characterized the SOT switching efficiency and effective fields in the SAF structures using harmonic Hall voltage technique. Additionally, a method to modulate the SOT fields by tuning the net magnetization of the SAF structures is shown. The antiferromagnetic alignment of the two FM layers generates the SOT fields of opposite signs. As such, the measured net SOT fields decrease when the magnitude of the upper layer magnetization (M_U) is close to that of the lower layer magnetization (M_L).

Antiferromagnetic coupling between two Co/Ni/Co tri-layers is attained by the insertion of a thin Ru layer via RKKY coupling. Three different SAF structures labeled as S1, S2 and S3 were chosen to explore the SOT phenomenon. The thin film stack structures of S1, S2 and S3 along with their measured magnetic properties are presented in Table 1. Shown in Fig. 1(a) are the out-of-plane hysteresis loops of the stacks measured by using vibrating sample magnetometer (VSM) technique. The perpendicular double switching in the hysteresis loops indicates the presence of antiferromagnetic RKKY coupling as well as perpendicular magnetic anisotropy (PMA) in all the samples S1, S2 and S3 [17]. The magnetization directions of the two ferromagnetic layers are represented by the direction of arrows. In the inset, a close-up of the hysteresis is inserted to compare remanent magnetization in the three samples. The remanent magnetization of the SAF stacks is tuned by varying thickness of a FM layer. Subsequently, the thin film stacks are patterned into 30 μm × 5 μm Hall-cross devices through electron beam lithography and Ar ion-milling. Scanning electron microscope (SEM) image of a device with the schematic of measurement configuration is shown in Fig. 1(b). Dimensions of the fabricated devices are kept identical for the three SAF stacks. Electrical characterization is performed on sample S1: Ta(3)/Pt(3)/[Co(0.4)/Ni(0.7)/Co(0.4)]/Ru(0.8)/[Co(0.4)/Ni(0.7)/Co(0.4)]/Ta(3). A small dc bias current of 1×10^9 A/m^2 is applied along the wire long axis (x- axis) to determine anomalous Hall resistance (R_{AHE}) as a function of magnetic field as shown in

Table 1
Magnetic properties of the synthetic antiferromagnetic thin films as measured from vibrating sample magnetometer (see supplementary).

Sample	Thin film stack	M_L (emu/cc)	M_U (emu/cc)	ΔM_S (emu/cc)	M_T (emu/cc)	H_c (Oe)	H_{ex} (Oe)	AFM RKKY peak
S1	Ta(3)/Pt(3)/[Co(0.4)/Ni(0.7)/Co(0.4)]/Ru (0.8)/[Co(0.4)/Ni(0.7)/Co(0.4)]/Ta(3)	660	330	165	495	310	6500	Second
S2	Ta(3)/Pt(3)/[Co(0.4)/Ni(0.7)/Co(0.4)]/Ru (0.8)/[(Co(0.4)/Ni(0.7))₂/Co(0.4)]/Ta(3)	635	345	20	460	1050	4500	Second
S3	Ta(3)/Pt(3)/[Co(0.4)/Ni(0.7)/Co(0.4)]/Ru (2.1)/ro(0.4)/Ni(0.7)/Co(0.4)]/Ta(3)	630	200	215	415	130	2500	Third

Fig. 1(c). The anomalous Hall resistance is a proxy of magnetization in a magnetic device and thus it can be used to identify the magnetization direction and switching between the two states. The R_{AHE} = Low (High) represents the Down (Up) magnetization state into the device. The square shaped R-H loop confirms the presence of perpendicular magnetic anisotropy corresponding to the minor loop of the SAF structure. Fig. 1(d) shows the R_{AHE} as a function of applied direct current (dc) in presence of a fixed longitudinal external magnetic field. The red and blue current-induced hysteresis loops correspond to H_x = +4000 Oe and H_x = −4000 Oe external magnetic fields, respectively. The arrows represent the switching direction of the SAF wire. The square hysteresis loops indicate that the magnetization of the SAF wire is completely switched by current between the two antiferromagnetic states. Here, we note that the favourable magnetization direction is reversed when the external magnetic field direction is changed from +x (red) to −x (blue). The current induced magnetization switching in the SAF structures is attributed to the SOT phenomenon [6]. Fig. 1(e) depicts the current-induced magnetization switching at various external magnetic fields. The critical current density for SOT switching drops linearly with increase in the external magnetic field as shown in Fig. 1(f). This behaviour is similar to that for PMA [24] and SAF wires [23]. Moreover, the current density required to switch the magnetization is about 2.3×10^{11} A/m², which is comparable to that for switching a single FM layer [24,25] as well as other SAF structures reported in the literature [22].

We employed AC harmonic Hall voltage measurements technique to estimate the SOT effective fields in the SAF structures. An alternating current of frequency ~333 Hz is injected into the Hall cross structures to induce magnetization oscillations. The amplitude of these oscillations depends on the magnitude and direction of the external magnetic field, and magnetic anisotropy of the device. The variation in first (V_ω) and second ($V_{2\omega}$) harmonics of the AHE voltage with in-plane external magnetic field is measured by using a lock-in-amplifier to detect the perturbations caused by the current on the magnetization. The in-plane magnetic field was swept between ± 2800 Oe along the longitudinal (H_L) and transverse (H_T) directions to the current, to quantify the Slonczewski-like (SL), and Field-like (FL) effective fields, respectively. The measurement schematics to determine the Slonczewski-like (H_{SL}) and Field-like (H_{FL}) effective fields are shown in Fig. 2(a) and (b), respectively. The following relationship is used to estimate the effective field values from the harmonic Hall voltage measurements [26,27]:

$$H_{SL(FL)} = -2\left(\frac{dV_{2\omega}}{dH_{L(T)}}\right)\bigg/\left(\frac{d^2V_\omega}{dH_{L(T)}^2}\right) \tag{1}$$

The results from macrospin model for current-induced magnetization switching in the SAF structures suggest that the SAF structures can be regarded as a single FM layer. The magnitude of net remnant magnetization of the SAF stacks is given by $(\Delta M_s) = M_L - M_U$, where M_L and M_U are lower and upper FM layer magnetizations, respectively [22]. Also, the magnetization of the SAF stack is assumed to be uniform and tilting in the magnetization with in-plane fields is not observed. A large change in the AHE voltage would be expected if the magnetization of SAF wires tilts by large angles in the direction of in-plane fields. However, in SAF stacks, strong RKKY coupling prevents the magnetization tilting in the direction of in-plane fields. Therefore, larger in-plane fields were needed to detect the magnetization oscillations and Eq. (1) can be used to calculate the SOT fields.

Fig. 2(c) and (d) show the variation in V_ω and $V_{2\omega}$ with H_L at a current density 1.04×10^{11} A/m². The measurements were performed for both net $M_Z > 0$ (net 'up' magnetization) and $M_Z < 0$ (net 'down' magnetization), shown by red and black curves, respectively. Fig. 2(e) and (f) are the plot of V_ω and $V_{2\omega}$ with H_T at a current density of 1.04×10^{11} A/m². The parabolic variation in the first harmonics voltage with the in-plane fields reveals that the net magnetization of the SAF stack remains constant during the field sweep. The second
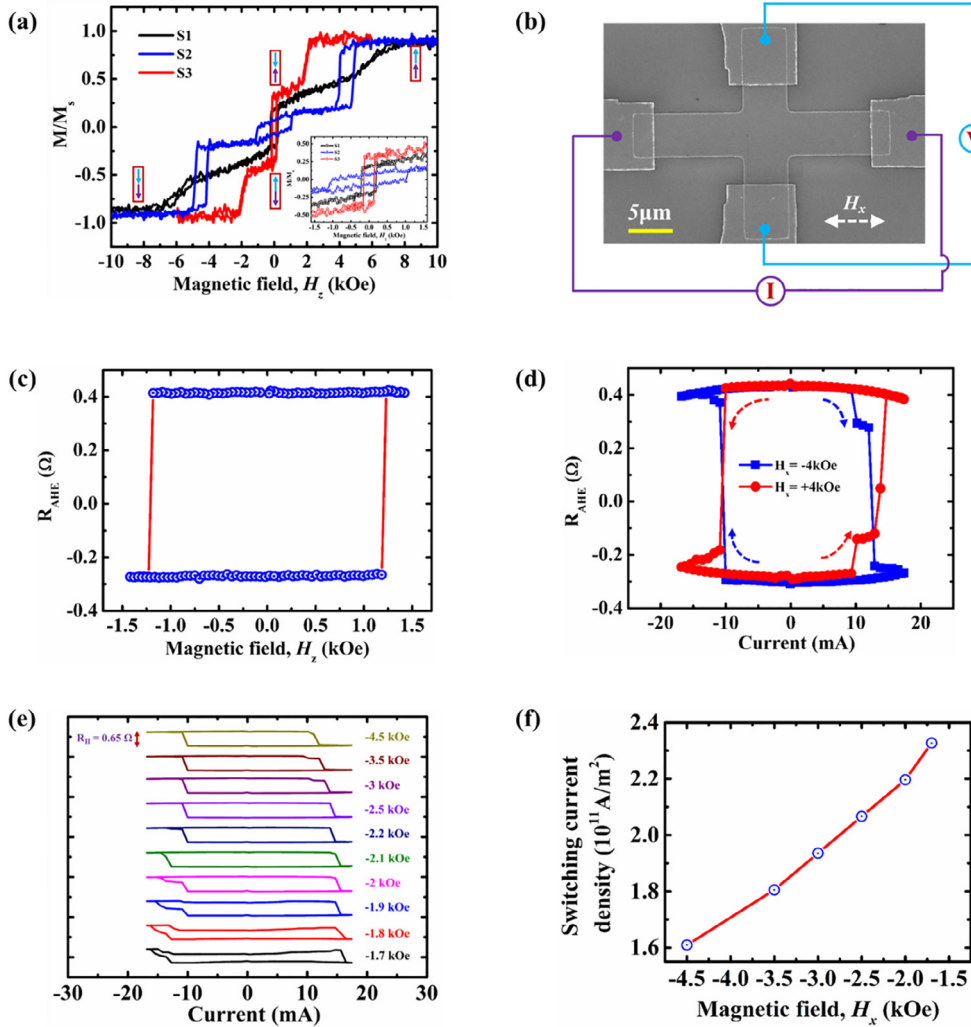
Fig. 1. (a) Out-of-plane hysteresis loops of the three SAF thin film stacks: S1 (black) – Ta(3)/Pt(3)/[Co(0.4)/Ni(0.7)/Co(0.4)]/Ru (0.8)/[Co(0.4)/Ni(0.7)/Co(0.4)]/Ta(3); S2 (blue) – Ta(3)/Pt(3)/[Co(0.4)/Ni(0.7)/Co (0.4)]/Ru(0.8)/{[Co(0.4)/Ni(0.7)]$_2$/Co (0.4)}/Ta(3); and S3 (red) – Ta(3)/Pt(3)/ [Co(0.4)/Ni(0.7)/Co(0.4)]/Ru(2.1)/[Co (0.4)/Ni(0.7)/Co(0.4)]/Ta(3). Numbers in parenthesis represent the layer thickness in 'nm'. The double switching behaviour in the measurement indicates the anti-ferromagnetic coupling between two magnetic trilayers: Co(0.4)/Ni(0.7)/Co(0.4) structures. Inset is the comparison of the net effective magnetization of the SAF stacks. (b) SEM image of the device with schematic circuit for harmonic measurements. (c) Anomalous Hall resistance (R_{AHE}) versus magnetic field loop of the device S1. The square shaped R-H loop confirms the presence of perpendicular magnetic anisotropy corresponds to the minor loop of the SAF stack S1. (d) Anomalous Hall resistance as a function of applied pulse currents in the presence of constant in-plane longitudinal magnetic fields $H_x = -4$kOe (blue) and $H_x = +4$kOe (red). The switching directions are also shown by dotted arrows for both the longitudinal field directions. (e) Current-induced magnetization switching in device S1 is characterized by anomalous Hall effect measurements under the various longitudinal magnetic fields. (f) Dependency of switching current density on the longitudinal magnetic field. (For interpretation of the references to colour in this figure legend, the reader is referred to the web version of this article.)

harmonic voltage varies monotonically with both H_L and H_T. However, the signs of the slopes are opposite for 'up' and 'down' magnetization states when the magnetic field is swept along the transverse direction. The SL-like and FL-like fields for various current densities extracted from the harmonic measurements, are plotted in Fig. 2(g) and (h), respectively.

The effective fields, H_{SL} and H_{FL} increase linearly with the applied current density for both 'up' (red) and down (black) net magnetization states as shown in Fig. 2(g) and (h), respectively. Also, it is noted that the magnitude of H_{SL} and H_{FL} is similar for 'up' and 'down' net magnetizations. However, sign of the H_{SL} is found to depend on the direction of the net magnetization, whereas, the sign of the H_{FL} is independent of the magnetization state. The longitudinal (β_L) and transverse (β_T) SOT efficiencies defined as H_{SL} and H_{FL} per 1×10^{11} A/m^2 current density, respectively, are calculated from the slope of the Fig. 2(g) and 2(h). The longitudinal (β_L) and transverse (β_T) SOT efficiencies for our SAF sample are found to be ~ 145 Oe/10^{11} A/m^2 and ~ 52 Oe/10^{11} A/m^2, respectively. However, the measured Hall resistance also contains the contributions from planar Hall effect (PHE) that leads to mixing of the H_{SL} and H_{FL}. Hence, we quantified the contribution of the PHE to accurately measure the SOT fields [10]. The contribution of PHE has been evaluated by measuring AHE at different field angles and a ratio of AHE to PHE resistance: $\xi = \Delta R_P / \Delta R_A \approx 0.33$ is obtained. Here, ΔR_A and ΔR_P are the AHE resistance and PHE resistance, respectively. The corrected H_{SL} and H_{FL} are calculated using following equations [26]:

$$Corr\_H_{SL} = \frac{H_{SL} + 2\xi H_{FL}}{1 - 4\xi^2}, \tag{2}$$

$$Corr\_H_{FL} = \frac{H_{FL} + 2\xi H_{SL}}{1 - 4\xi^2}, \tag{3}$$

The PHE corrected longitudinal (Corr_H_{SL}) and transverse (Corr_H_{FL}) fields, together with H_{SL} and H_{FL} are plotted as a function of current density in Fig. 3(a). The corrected effective fields increase linearly with the applied current density. The Corr_H_{SL} and Corr_H_{FL} per 1×10^{11} A/m^2 current density are found to be ~ 320 Oe and ~ 260 Oe, respectively. The ratios of H_{SL} to H_{FL} with and without PHE corrections with the current density are plotted in Fig. 3(b) and the contribution of PHE in SOT-induced effectives fields cannot be neglected in the SAF thin films.

To gain insight on the effect of magnetization on the SOT fields, the harmonic Hall measurements were repeated on the Hall cross structure patterned from SAF stack S2. In S2, the magnetization of the upper FM layer is varied by changing the thickness of the top layer while keeping the bottom layer thickness same as S1. In the SAF stack, magnetization of the two FM layers is coupled in opposite direction via an ultra-thin Ru layer. Ideally, the sample S1 should possess no net magnetization, however the measurements reveal a finite net magnetization, even though both FM layers were composed of identical material composition and thicknesses. The net magnetization in the SAF thin film stacks can be attributed to the Pt underlayer that provides better crystallinity and promotes stronger PMA for bottom FM layer while the upper FM layer which is grown on Ru has weaker PMA. The number of [Co/Ni]
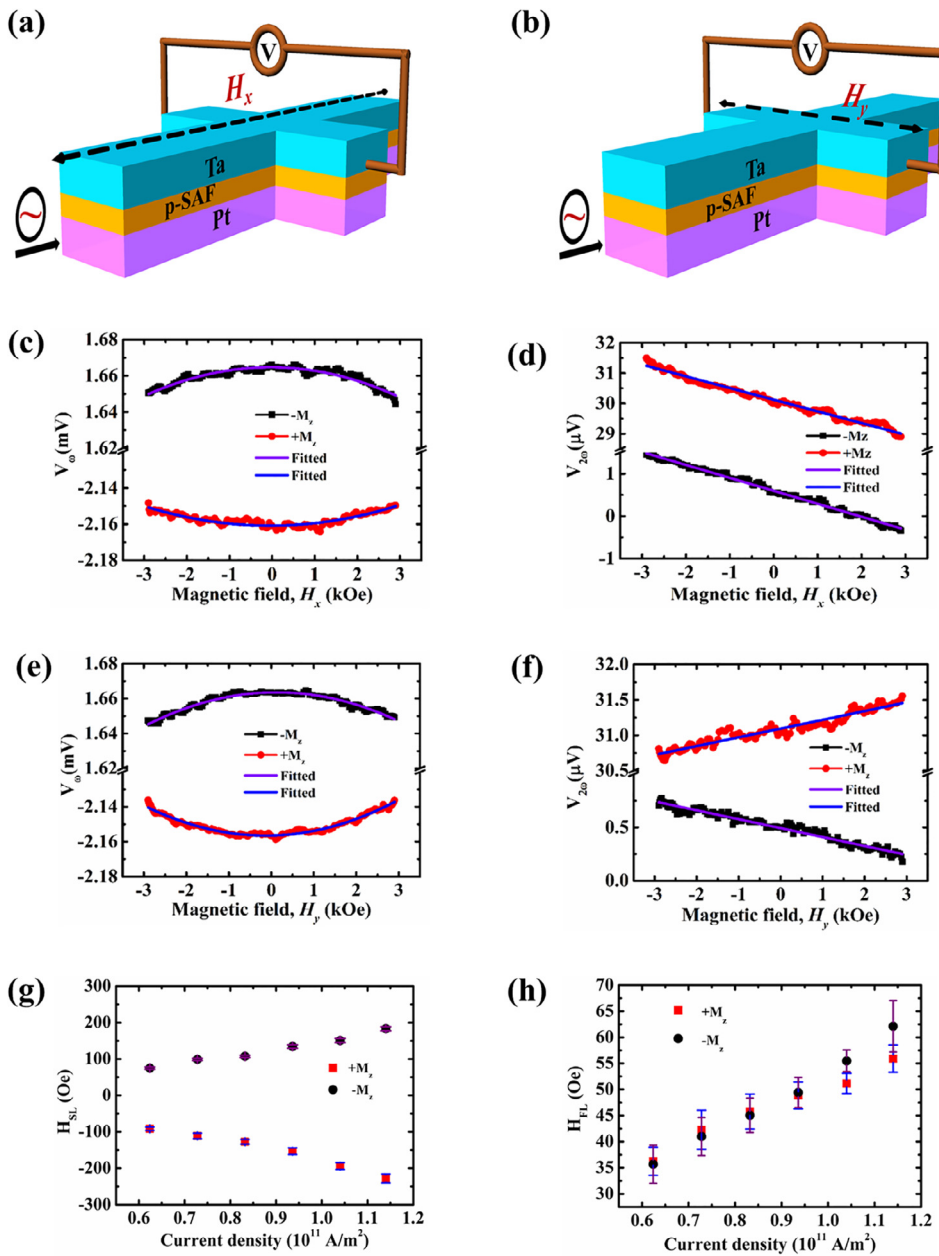
Fig. 2. Schematics of experimental circuit geometry to measure (a) Slonczewski-like and (b) field-like effective fields in SAF structures with perpendicular magnetic anisotropy (p-SAF). (c) First and (d) second harmonics of the Hall voltage for net 'up' (red) and 'down' (black) magnetizations versus longitudinal field, measured for a current density 1.04×10^{11} A/m^2. (e) First and (f) second harmonics of the Hall voltage for net 'up' (red) and 'down' (black) magnetizations versus transverse field, measured for a current density 1.04×10^{11} A/m^2. (g) SL fields for 'up' (red) and 'down' (black) net magnetizations with current densities. (h) FL fields for 'up' (red) and 'down' (black) net magnetizations with different current densities. All the measurements were performed on the device fabricated on thin film stack S1. (For interpretation of the references to colour in this figure legend, the reader is referred to the web version of this article.)

repetitions in the upper layer are increased to magnify the upper layer magnetization that reduces the net magnetization of SAF stack as shown by the blue hysteresis in the Fig. 1(a). The thin film stack of the sample S2 is: Ta(3)/Pt(3)/[Co(0.4)/Ni(0.7)/Co(0.4)]/Ru(0.8)/{[Co(0.4)/Ni(0.7)]$_2$/Co(0.4)}/Ta(3). The Ru thickness is increased to obtain

the third RKKY antiferromagnetic coupling in sample S3 that reduces antiferromagnetic coupling strength and magnetization of the upper FM layer. The thin film stack of the sample S3 is: Ta(3)/Pt(3)/[Co(0.4)/Ni(0.7)/Co(0.4)]/Ru(2.1)/[Co(0.4)/Ni(0.7)/Co(0.4)]/Ta(3). The magnetization of lower and upper FM layers for sample S1, S2 and S3 is listed
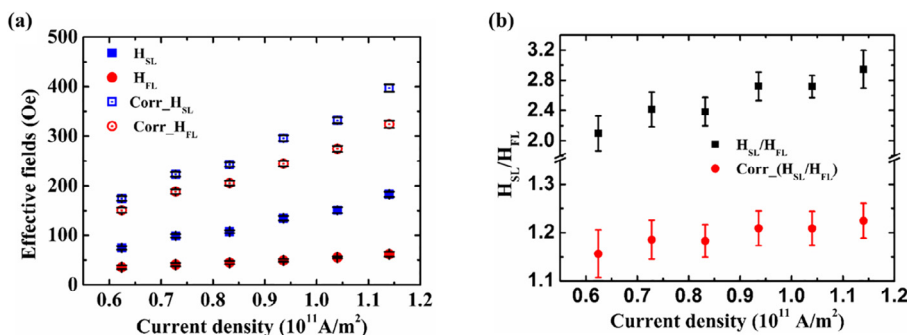

Fig. 3. (a) The SL (blue squares) and FL (red circles) effective fields without (solid) and with (open) planar Hall effect (PHE) corrections for sample S1 at different current densities. (b) The ratio of H_{SL} to H_{FL} without (black) and with (red) PHE correction at different current densities. (For interpretation of the references to colour in this figure legend, the reader is referred to the web version of this article.)
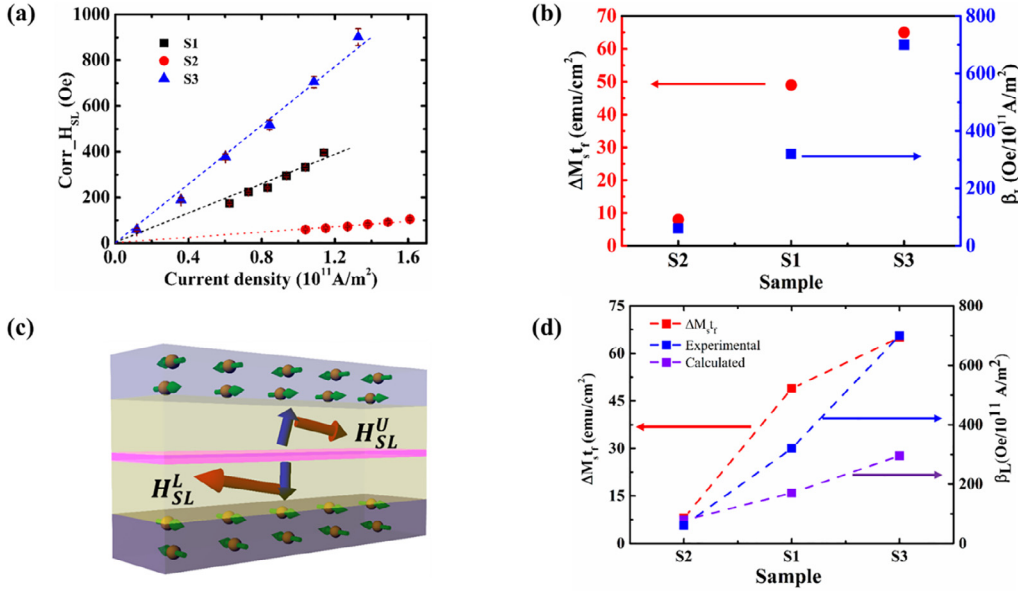
Fig. 4. (a) The SL effective fields for sample S1, S2 and S3 with current densities. (b) Longitudinal SOT efficiencies (β_L) (blue) and the areal net magnetization (red) for sample S1, S2 and S3. (c) Schematic diagram to illustrate the magnetization of the ferromagnetic layers, spin accumulations at the ferromagnetic/heavy-metal interfaces and the SL field directions in the upper and lower FM layers. (d) Experimentally observed (blue) and calculated (violet) longitudinal SOT efficiencies (β_L) together with the net areal magnetization (red) for sample S1, S2 and S3. (For interpretation of the references to colour in this figure legend, the reader is referred to the web version of this article.)

in Table 1.

Harmonic Hall measurements were conducted on sample S2 and S3 to obtain the SOT- fields. The contribution from the PHE in the AHE is quantified and the corrected SL fields are plotted with the current density in Fig. 4(a). The SL fields increase linearly with the current densities for all the samples as expected. The longitudinal SOT efficiencies or H_{SL} per 1×10^{11} A/m^2 current density (β_L) are shown by the blue squares in Fig. 4(b). The SOT induced longitudinal effective (H_{SL}) can be written as [28]

$$\overrightarrow{H}_{SL} = -\frac{\hbar \theta_{SH} J}{2 |e| \Delta M_s t_f} \widehat{m} \times \widehat{y}, \tag{4}$$

where, 'θ_{SH}' is the effective spin Hall angle, 'J' is the applied current density, 'e' is the electron charge, 'ΔM_s' is the net magnetization of the SAF stack, 't_f' is the FM thin film thickness, and $\widehat{m}$ and $\widehat{y}$, are the unit vectors along the magnetization and y-directions, respectively. The spin Hall angle is the ratio of the spin-current to the charge current in a HM layer. In the SAF stacks S1, S2 and S3, the HM layers were kept identical to investigate the effect of the net magnetization on the SL fields. Therefore, the effective spin Hall angle of all the samples can be considered comparable and the H_{SL} only depends on the product of net magnetization and FM layer thickness i.e. $\Delta M_s t_f$. The $\Delta M_s t_f$ and the longitudinal SOT efficiencies for three samples are plotted in Fig. 4(b) in red and blue, respectively. Fig. 4(b) shows that the β_L is directly proportional to the $\Delta M_s t_f$ which is in contrast with already reported experimental results for PMA structures and Eq. (4) [28]. The SOT fields in SAF structure increases with areal magnetization of the SAF, whereas in PMA nanowires the SOT fields are reported to be inversely proportional to the magnetization [27]. To understand how the SOTs are generated in the SAF structures, we define the solitary longitudinal SOT fields for the upper (H_{SL}^U) and the lowers (H_{SL}^L) FM layers as

$$\overrightarrow{H}_{SL}^U = -\frac{\hbar \theta_{SH}^U J}{2 |e| M_s^U t_f^U} \widehat{m}^U \times \widehat{y}, \tag{5}$$

$$\overrightarrow{H}_{SL}^L = -\frac{\hbar \theta_{SH}^L J}{2 |e| M_s^L t_f^L} \widehat{m}^L \times \widehat{y}, \tag{6}$$

Here, θ_{SH}^U and θ_{SH}^L are the net effective spin Hall angles for the upper FM layer – Ru/FM/Ta and the lower FM layer- Pt/FM/Ru, respectively. The spin Hall angle of Pt (θ_{SH}^{Pt}) = +0.11 and and Ta (θ_{SH}^{Ta}) = −0.25 are from our previous work [11,29,30]. The spin Hall angle of Ru (θ_{SH}^{Ru}) = +0.04 [31] is reported in the literature. Even though Ru is a bad spin-current generator, however, large spin-orbit torques has been

reported in Pt/FM/Ru hetero-structures due to spin-current absorption at FM-Ru interface. Moreover, this spin-current absorption based theory could only explain the experimental results qualitatively [31]. We approximate the spin Hall angles for upper and lower FM layer as: $\theta_{SH}^U = \theta_{SH}^{Ru} - \theta_{SH}^{Ta} = 0.29$ and $\theta_{SH}^L = \theta_{SH}^{Pt} - \theta_{SH}^{Ru} = 0.07$ [6,10,11,30–32]. The saturation magnetization of the lower (M_s^L) and upper (M_s^U) layers are listed in Table 1. The thicknesses of the upper and lower FM layers are 't_f^U' and 't_f^L', respectively. The experimentally measured net longitudinal SOT field of the SAF stack (H_{SL}^T) therefore, can be written as the vector sum of the longitudinal SOT fields of upper (H_{SL}^U) and lowers (H_{SL}^L) layer:

$$\overrightarrow{H}_{SL}^T = \overrightarrow{H}_{SL}^U + \overrightarrow{H}_{SL}^L = -\frac{\hbar \theta_{SH}^U J}{2 |e| M_s^U t_f^U} \widehat{m}^U \times \widehat{y} - \frac{\hbar \theta_{SH}^L J}{2 |e| M_s^L t_f^L} \widehat{m}^L \times \widehat{y}, \tag{7}$$

For a positive saturation of the SAF stack, $\widehat{m}^U = +\widehat{z}$, and $\widehat{m}^L = -\widehat{z}$. Therefore,

$$\overrightarrow{H}_{SL}^T = \frac{\hbar J}{2 |e|} \left(\frac{\theta_{SH}^U}{M_s^U t_f^U} - \frac{\theta_{SH}^L}{M_s^L t_f^L} \right) \widehat{x} \tag{8}$$

$$\overrightarrow{H}_{SL}^T \propto \frac{M_s^L t_f^L - M_s^U t_f^U}{M_s^U t_f^U M_s^L t_f^L} \widehat{x} \tag{9}$$

The magnitude of the SOT fields in the SAF structures is proportional to the net areal magnetization of the stack as observed in the experiments. The effective spin Hall angles for the top and bottom FM layers were identical in the sign but the magnetization directions were antiparallel to each other. Therefore, the SOT fields from the lower and upper FM layers were opposite in the direction and the measured net effective fields ($\overrightarrow{H}_{SL}^T$) are the vector sum of the SOT fields generated from the two FM layers. The directions of the effective fields in the SAF structure are shown by a schematic in Fig. 4(c). The experimentally observed and the calculated net effective fields from our approximation together with the net areal magnetization for S1, S2 and S3 are plotted in Fig. 4(d). The calculated SOT fields using Eq. (8), show the same trend as of the observed in experiments. The SOT fields increase with the net areal magnetization of the SAF structure as expected from Eq. (8).

To compare the SOT fields in all three SAF samples, the lower FM layer and the HM layers were kept identical and magnetization of the upper FM layer was varied. The SOT field generated by the lower FM

layer is along the $-x$ direction as shown in Fig. 4(c). The upper FM layer in the SAF structure generates higher SOT field along the $+x$ direction as: it is interfaced with material that have higher spin Hall angle (θ_{SH}^U=0.29) and contains less M_s^U values as grown on the Ru (see Eq. (5)). Therefore, the direction of net SOT field was along the direction of the SOT field generated by upper FM layer. For sample S1, S2 and S3, the observed β_L values are ~320 Oe, 60 Oe and 700 Oe, respectively. The smaller SOT fields in sample S2 can be attributed to the fact that the areal magnetization ($M_s^U t_f^u$) of upper and lower FM layers are similar in the magnitude as can be seen in the inset of Fig. 1(a). The effective fields from upper and lower FM layer were cancelled out and lesser net SOT fields were observed. While in S3, the higher net areal magnetization ($M_s^U t_f^u - M_s^L t_f^L$) produced higher net SOT fields. Our analysis show that the observed SOT fields are the vector sum of the individual SOT fields in the lower and upper layers of a SAF stack and are in qualitative agreement with the calculated values. However, quantitatively the calculated SOT fields are smaller than the experimentally measured values. Recent experimental results have shown that the SOT strength can be largely enhanced by transverse spin-current absorption in a FM layer due to FM/Ru interface [31]. The absorption of transverse spin-currents in the FM layers is found to be proportional to the thickness of the FM layers. In addition, the spin dephasing length is found to be 1.2 ± 1 nm in the layered FM structures [33]. In our calculations the effect of the spin absorption in the FM layers is not considered and thus the calculated values are not in quantitative agreement with the experimental values. The difference in the calculated and the experimental SOT field values is more obvious in the sample S1 and S3 compared to the sample S2. The upper FM layer in the sample S2 has the thickness (~2.6 nm) twice of the spin dephasing length (~1.2 ± 1 nm) that hindered the spin absorption and therefore, the SOT fields. The higher SOT fields in S1 and S3 could be attributed to the fact that thicknesses of the FM layers (1.5 nm) are in close proximity to the spin dephasing length (1.2 ± 1 nm). Therefore, the effect of enhanced spin-absorption cannot be neglected in the S1 and S3. While our simple approximation qualitatively explains the experimental results, the origin of large SOT fields in the SAF stacks requires a detailed theoretical calculation considering the spin absorption at the FM/Ru interface combined with the complicated interfacial structure.

In conclusion, we have shown that in-plane charge currents in HM can be used to manipulate the magnetization of an adjacent SAF layer by making use of spin-orbit torques. The efficient magnetization switching was achieved in the SAF structures, even though the two FM layers were coupled via strong antiferromagnetic coupling. The SOT fields in the SAF structures were quantified by using AC harmonic Hall measurements technique. Contrary to PMA structures, the measured SOT effective fields in the SAF structures are found to increase with the net magnetization. The SOT fields are modulated by tuning the areal magnetization of the SAF structures. Furthermore, a simple approach is proposed to calculate the SOT fields in the SAF structures which indicates that the SOT fields in the SAF structures can be approximated from the vector sum of the individual SOT fields generated from the two FM layers. The proposed method for the SOT-induced effective field estimations in the SAF structure will be helpful in understanding the underlying physics of magnetization switching and designing of domain wall and skyrmion based memory and logic devices.

Acknowledgment

References

[1] S.S.P. Parkin, M. Hayashi, L. Thomas, Magnetic domain-wall racetrack memory, Science 320 (2008) 190–195, https://doi.org/10.1126/science.1145799.

[2] P. Sethi, C. Murapaka, G.J. Lim, W.S. Lew, In-plane current induced domain wall nucleation and its stochasticity in perpendicular magnetic anisotropy Hall cross structures, Appl. Phys. Lett. 107 (2015) 192401, , https://doi.org/10.1063/1.4935347.

[3] Z. Diao, Z. Li, S. Wang, Y. Ding, A. Panchula, E. Chen, L.C. Wang, Y. Huai, Spin-transfer torque switching in magnetic tunnel junctions and spin-transfer torque random access memory, J. Phys. Condens. Matter. 19 (2007) 165209, , https://doi.org/10.1088/0953-8984/19/16/165209.

[4] C. Murapaka, P. Sethi, S. Goolaup, W.S. Lew, Reconfigurable logic via gate controlled domain wall trajectory in magnetic network structure, Sci. Rep. 6 (2016) 20130, https://doi.org/10.1038/srep20130.

[5] L. Liu, O.J. Lee, T.J. Gudmundsen, D.C. Ralph, R.A. Buhrman, Current-induced switching of perpendicularly magnetized magnetic layers using spin torque from the spin hall effect, Phys. Rev. Lett. 109 (2012) 096602, , https://doi.org/10.1103/PhysRevLett.109.096602.

[6] L. Liu, C.F. Pai, Y. Li, H.W. Tseng, D.C. Ralph, R.A. Buhrman, Spin-torque switching with the giant spin hall effect of tantalum, Science (80-.) 336 (2012) 555–558, https://doi.org/10.1126/science.1218197.

[7] I.M. Miron, G. Gaudin, S. Auffret, B. Rodmacq, A. Schuhl, S. Pizzini, J. Vogel, P. Gambardella, Current-driven spin torque induced by the Rashba effect in a ferromagnetic metal layer, Nat. Mater. 9 (2010) 230–234, https://doi.org/10.1038/nmat2613.

[8] I.M. Miron, T. Moore, H. Szambolics, L.D. Buda-Prejbeanu, S. Auffret, B. Rodmacq, S. Pizzini, J. Vogel, M. Bonfim, A. Schuhl, G. Gaudin, Fast current-induced domain-wall motion controlled by the Rashba effect, Nat. Mater. 10 (2011) 419–423, https://doi.org/10.1038/nmat3020.

[9] F. Luo, S. Goolaup, W.C. Law, S. Li, F. Tan, C. Engel, T. Zhou, W.S. Lew, Simultaneous determination of effective spin-orbit torque fields in magnetic structures with in-plane anisotropy, Phys. Rev. B. 95 (2017) 174415, , https://doi.org/10.1103/PhysRevB.95.174415.

[10] S. Woo, M. Mann, A.J. Tan, L. Caretta, G.S.D. Beach, Enhanced spin-orbit torques in Pt/Co/Ta heterostructures, Appl. Phys. Lett. 105 (2014) 212404, , https://doi.org/10.1063/1.4902529.

[11] P. Sethi, S. Krishnia, S.H. Li, W.S. Lew, Modulation of spin-orbit torque efficiency by thickness control of heavy metal layers in Co/Pt multilayers, J. Magn. Magn. Mater. 426 (2017) 497–503, https://doi.org/10.1016/j.jmmm.2016.11.130.

[12] Y.W. Oh, S.H.C. Baek, Y.M. Kim, H.Y. Lee, K.D. Lee, C.G. Yang, E.S. Park, K.S. Lee, K.W. Kim, G. Go, J.R. Jeong, B.C. Min, H.W. Lee, K.J. Lee, B.G. Park, Field-free switching of perpendicular magnetization through spin-orbit torque in antiferromagnet/ferromagnet/oxide structures, Nat. Nanotechnol. 11 (2016) 878–884, https://doi.org/10.1038/nnano.2016.109.

[13] S. Fukami, C. Zhang, S. Duttagupta, A. Kurenkov, H. Ohno, Magnetization switching by spin-orbit torque in an antiferromagnet-ferromagnet bilayer system, Nat. Mater. 15 (2016) 535–541, https://doi.org/10.1038/nmat4566.

[14] C. Engel, S. Goolaup, F. Luo, W. Gan, W.S. Lew, Spin-orbit torque induced magnetization anisotropy modulation in Pt/(Co/Ni)4/Co/IrMn heterostructure, J. Appl. Phys. 121 (2017) 143902, , https://doi.org/10.1063/1.4980108.

[15] A. Van Den Brink, G. Vermijs, A. Solignac, J. Koo, J.T. Kohlhepp, H.J.M. Swagten, B. Koopmans, Field-free magnetization reversal by spin-Hall effect and exchange bias, Nat. Commun. 7 (2016) 10854, https://doi.org/10.1038/ncomms10854.

[16] W.L. Gan, S. Krishnia, W.S. Lew, Efficient in-line skyrmion injection method for synthetic antiferromagnetic systems, New J. Phys. 20 (2018) 013029, , https://doi.org/10.1088/1367-2630/aaa113.

[17] S.H. Yang, K.S. Ryu, S. Parkin, Domain-wall velocities of up to 750 m s-1driven by exchange-coupling torque in synthetic antiferromagnets, Nat. Nanotechnol. 10 (2015) 221–226, https://doi.org/10.1038/nnano.2014.324.

[18] S. Krishnia, P. Sethi, W.L. Gan, F.N. Kholid, I. Purnama, M. Ramu, T.S. Herng, J. Ding, W.S. Lew, Role of RKKY torque on domain wall motion in synthetic antiferromagnetic nanowires with opposite spin Hall angles, Sci. Rep. 7 (2017) 11715, https://doi.org/10.1038/s41598-017-11733-9.

[19] X. Zhang, Y. Zhou, M. Ezawa, Magnetic bilayer-skyrmions without skyrmion Hall effect, Nat. Commun. 7 (2016) 10293, https://doi.org/10.1038/ncomms10293.

[20] D.C. Worledge, G. Hu, D.W. Abraham, J.Z. Sun, P.L. Trouilloud, J. Nowak, S. Brown, M.C. Gaidis, E.J. O'Sullivan, R.P. Robertazzi, Spin torque switching of perpendicular Ta|CoFeB|MgO-based magnetic tunnel junctions, Appl. Phys. Lett. 98 (2011) 96–99, https://doi.org/10.1063/1.3536482.

[21] L. Cuchet, B. Rodmacq, S. Auffret, R.C. Sousa, I.L. Prejbeanu, B. Dieny, Perpendicular magnetic tunnel junctions with a synthetic storage or reference layer: A new route towards Pt-and Pd-free junctions, Sci. Rep. 6 (2016) 21246, https://doi.org/10.1038/srep21246.

[22] C. Bi, H. Almasi, K. Price, T. Newhouse-Illige, M. Xu, S.R. Allen, X. Fan, W. Wang, Anomalous spin-orbit torque switching in synthetic antiferromagnets, Phys. Rev. B 95 (2017) 104434, , https://doi.org/10.1103/PhysRevB.95.104434.

[23] G.Y. Shi, C.H. Wan, Y.S. Chang, F. Li, X.J. Zhou, P.X. Zhang, J.W. Cai, X.F. Han, F. Pan, C. Song, Spin-orbit torque in MgO/CoFeB/Ta/CoFeB/MgO symmetric structure with interlayer antiferromagnetic coupling, Phys. Rev. B 95 (2017) 104435, , https://doi.org/10.1103/PhysRevB.95.104435.

[24] J. Yu, X. Qiu, W. Legrand, H. Yang, Large spin-orbit torques in Pt/Co-Ni/W heterostructures, Appl. Phys. Lett. 109 (2016) 042403, , https://doi.org/10.1063/1.4959958.

[25] C. Bi, L. Huang, S. Long, Q. Liu, Z. Yao, L. Li, Z. Huo, L. Pan, M. Liu, Thermally

assisted magnetic switching of a single perpendicularly magnetized layer induced by an in-plane current, Appl. Phys. Lett. 105 (2014) 022407, , https://doi.org/10.1063/1.4890539.

[26] M. Hayashi, J. Kim, M. Yamanouchi, H. Ohno, Quantitative characterization of the spin-orbit torque using harmonic Hall voltage measurements, Phys. Rev. B 89 (2014) 144425, , https://doi.org/10.1103/PhysRevB.89.144425.

[27] J. Kim, J. Sinha, M. Hayashi, M. Yamanouchi, S. Fukami, T. Suzuki, S. Mitani, H. Ohno, Layer thickness dependence of the current-induced effective field vector in Ta|CoFeB|MgO, Nat. Mater. 12 (2013) 240–245, https://doi.org/10.1038/nmat3522.

[28] A.V. Khvalkovskiy, V. Cros, D. Apalkov, V. Nikitin, M. Krounbi, K.A. Zvezdin, A. Anane, J. Grollier, A. Fert, Matching domain-wall configuration and spin-orbit torques for efficient domain-wall motion, Phys. Rev. B – Condens. Matter Mater. Phys. 87 (2013) 020402, , https://doi.org/10.1103/PhysRevB.87.020402.

[29] M. Ramu, S. Goolaup, W.L. Gan, S. Krishnia, G.J. Lim, W.S. Lew, Spin orbit torque induced asymmetric depinning of chiral Néel domain wall in Co/Ni

heterostructures, Appl. Phys. Lett. 110 (2017) 162402, , https://doi.org/10.1063/1.4980120.

[30] P. Sethi, S. Krishnia, W.L. Gan, F.N. Kholid, F.N. Tan, R. Maddu, W.S. Lew, Bi-directional high speed domain wall motion in perpendicular magnetic anisotropy Co/Pt double stack structures, Sci. Rep. 7 (2017) 4964, https://doi.org/10.1038/s41598-017-05409-7.

[31] X. Qiu, W. Legrand, P. He, Y. Wu, J. Yu, R. Ramaswamy, A. Manchon, H. Yang, Enhanced spin-orbit torque via modulation of spin current absorption, Phys. Rev. Lett. 117 (2016) 217206, , https://doi.org/10.1103/PhysRevLett.117.217206.

[32] S. Emori, U. Bauer, S.M. Ahn, E. Martinez, G.S.D. Beach, Current-driven dynamics of chiral ferromagnetic domain walls, Nat. Mater. 12 (2013) 611–616, https://doi.org/10.1038/nmat3675.

[33] A. Ghosh, S. Auffret, U. Ebels, W.E. Bailey, Penetration depth of transverse spin current in ultrathin ferromagnets, Phys. Rev. Lett. 109 (2012) 127202, , https://doi.org/10.1103/PhysRevLett.109.127202.